Draft version May 15, 2015
Preprint typeset using LaTeX style emulateapj v. 12/16/11

SEARCHING FOR ACTIVE ASTEROIDS USING THE OUTER SOLAR SYSTEM OBJECT SURVEY

Kristi Webb
University of Victoria
Draft version May 15, 2015

ABSTRACT

The Outer Solar System Object Survey was used to search for active asteroid candidates. A test sample of 90 observations of the Hungaria asteroid family, previously discovered active asteroids, and a comet discovered but unreported in the Canada-France Ecliptic Plane Survey was chosen to analyze the success of the developed search pipeline. Each object was first examined to determine its precise location on the respective exposure, then the brightness profile was measured from the objects' PSF. The profile was compared against that of a stellar model, where the residuals being larger than a lower limit of 3 sigma indicated activity around the asteroid. From the test sample only 62 asteroids could be compared with a stellar model, 9 of which required visual inspection as the precise location could not be determined by the photometry software. Of the 62, 53 (85.4%) were retained to be analyzed by the above methods. No asteroids or previously discovered active asteroids in this survey indicated comet-like activity, each comet was found to deviate by the stellar model by more than 5 sigma.
The pipeline developed in this study is available open-source (https://github.com/k-a-webb/MainBeltComets).

Keywords: Active asteroids, Main belt comets, Outer Solar System Object Survey (OSSOS)

1. INTRODUCTION

Prior to the last decade, comets and asteroids have been thought of as separate populations differing in both morphology and dynamics. As each population has different fractions of volatile content, an obvious distinction is the presence of a transient coma and/or tail around a comet, whereas asteroids exhibit bare nuclei photometric properties. With the recent advent of large wide-field surveys which have regularly monitored large populations of solar system bodies, objects which exist between the classification of comets and asteroids have been discovered. The classical view of comets being rocky *ice* bodies with highly eccentric orbits, and asteroids being icy *rock* bodies with stable orbits confined to the main asteroid belt between Mars and Jupiter, has been supplanted by the discovery of comet-asteroid transition objects (Sheppard and Trujillo 2015). Asteroids in comet-like orbits, dynamically asteroidal objects that exhibit burst of cometary activity or are associated with meteor streams such as the Damocloids (Gilbert and Wiegert (2009), Sonnett et al. 2011; and references therein) exist between the accustomed classification criteria. These objects may be comets which have exhausted their volatile content or are dormant, or asteroids which have a higher volatile fraction. This study focuses on the 'active asteroids' (AAs), also known as main belt comets (MBCs), which are a population of bodies with stable asteroid-like main belt orbits that exhibit transient mass loss forming comae and/or tails consistent with cometary morphology (Hsieh and Jewitt 2006).

It is expected that icy objects in the inner solar system would have sublimated on timescales of the order of the age of the Solar System. As such, the AAs pose an interesting insight to the heliocentric distance at which ice condenses, known as the 'snow line', which of interest to planetary formation and determining the chemistry of the early solar nebula. For objects which formed in the the outer region of the main belt, the water ice which was present at the time of formation and not exposed to primordial heating may still remain in reservoirs beneath the surface (Prialnik and Rosenberg 2009). According to models developed by Fanale and Salvail (1989), beyond heliocentric distances of 2.4 AU ice can be protected against sublimation by a relatively thin surface regolith of depth 1 – 100 m for the entire age of the solar system. If the ice layer were to be exposed to sub solar heating by an impact or other triggering event, sublimation could eject dust particles from the surface. The cause of the dust emission may be different for each object and could include ice sublimation, impact ejecta, rotational instabilities due to YORP (Yarkovsky-O'Keefe-Radzievskii-Paddack) torques, or a combination of several effects (Jewitt et al. 2015; and references therein).

Since the first discovery of an active main-belt asteroid, 133P/Elst-Pizarro (Elst et al. 1996), several attempts have been made to identify new objects of this type. There have been 19 AAs identified at the time of this study, with diverse set of orbital dynamics (see figure 1) (Jewitt et al. 2015; Hsieh et al. 2015). A comprehensive review of these surveys can be found in Hsieh et al. (2015). A persistent challenge to this effort is that the detection of the faint coma or tails around small dark objects is highly dependent on the magnitude constraints of the survey. As most asteroids fall near the limiting magnitude of the survey in which they are discovered, as a result of the steep size population distribution of the asteroid population (Jewitt et al. 2015), objects which are larger, closer, or have higher albedo are preferentially detected and any dust emission would be more easily apparent. At present, the active fraction of identified AAs greater than 1 km to main belt asteroids greater than 1 km is approximated as $f \sim 10^5$, and describes a strong lower limit as many objects are yet undetected (Jewitt et al. 2015).

In this paper, a study of main belt objects observed

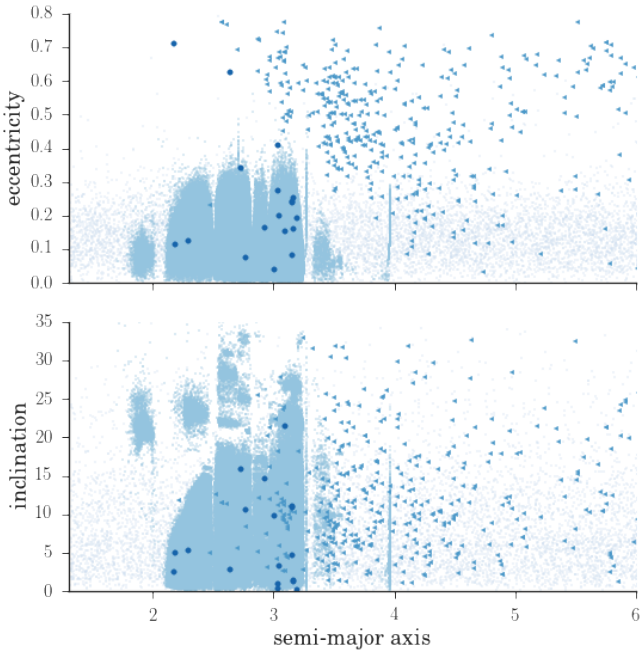

Figure 1. In order of increasing colour intensity, all of the solar system objects as catalogued by the Minor Planet Centre (MPC) together with the numbered asteroids catalogued by the Astronomical Dynamics site (AstDys), the known comets, and previously discovered AAs, are shown with their inclination and eccentricity as a function of semi-major axis (**?**Agency et al. 2015). It is apparent the the AAs share a dynamical orbit with the asteroid population. As a sub-population, the AAs do not share a well defined orbital phase space but are rather dispersed in terms of semi-major axis, eccentricity, and inclination.

by the Canada-France-Hawaii Telescope (CFHT) Outer Solar System Origins Survey (OSSOS) is presented to search for evidence of cometary-like activity in asteroidal bodies. Previously undetectable emission activity may be able to be identified in the OSSOS survey, which has a limiting magnitude much fainter than previous surveys ($\lesssim 22$ mag in the r band). Potential activity is identified by measuring the asteroids' brightness profile and comparing it to a stellar model profile of the same magnitude in order to detect a large deviation in width, potentially characteristic of a coma or jet. Asteroids which have residuals larger than a 3 sigma deviation are subjected to visual examination. This is similar to the process employed by Luu (1992), Sonnett et al. (2011), and Gilbert and Wiegert (2009).

2. OBSERVATIONS

The OSSOS observations were taken with the MegaPrime camera, a wide-field optical camera on the CFHT, located at the summit of Mauna Kea, Hawaii. The observations began in February 2013 and will continue until 2017. The image plane is a collection of 36 CCDs, each 2048 x 4125 CCD with resolution of 0.185"/pix. This covers a field of approximately one square degree on the sky. Each block of data taken consists of a mosaic of 21 segments of one-square-degree sky coverage, and at present, covers two orbital phase spaces on the plane of the ecliptic, and two off plane at low inclinations. The OSSOS survey employs the u* and r' filters on the MegaCam with integration times of 287, 387, and 500 seconds, yielding a lower limit of $m_r \sim$ 24.5 magnitudes.

The OSSOS images were pre-processed by standard data detrending with the MegaPipe image stacking pipeline. An astrometric solution was applied by (Bannister et al. 2015). Flux source characteristic measurements were obtained from a python wrapper for Source Extractor (Bertin and Arnouts 1996), Source Extraction and Photometry in Python (SEP) (Barbary and contributers 2015), and were used to extract the photometric properties.

The survey covers a wide field of both the ecliptic plane and low inclinations allowing for the observation of a large number of main belt objects in various orbital phase spaces, see Figures 2,3. As the observations were not targeted to specific main-belt populations, OSSOS provides a broad sample of the asteroid population both in terms of orbital dynamics and population density (see figure 4). This then allows for a determination of the upper-limit of AAs expected for the entire main-belt.

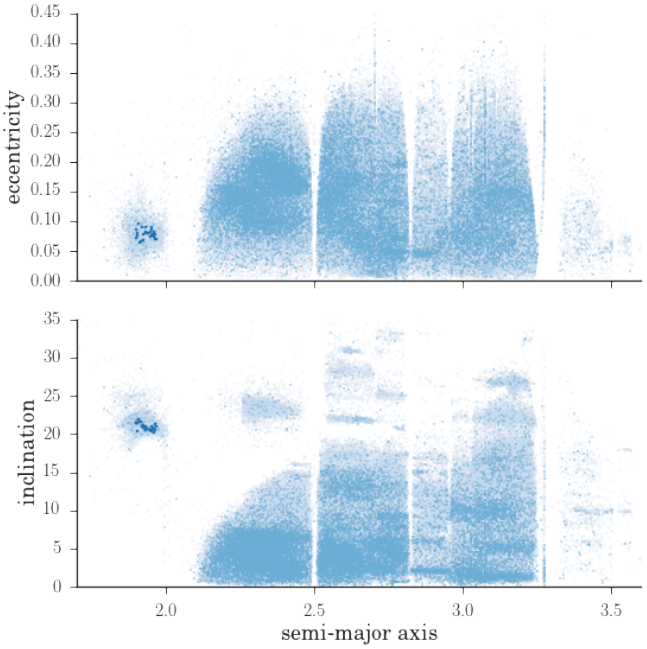

Figure 2. In order of increasing colour intensity, the numbered asteroids are shown with the asteroids observed by OSSOS, as well as the Hungaria family selected as a test sample, with inclination and eccentricity as a function of semi-major axis. The asteroid population is seen to be well sampled by the OSSOS survey in terms of orbital phase space.

3. ANALYSIS

Three test groups were selected to ensure the efficiency of our search. The first is the Hungaria family, which is a population of bodies in the inner edge of the main asteroid belt at relatively high inclination and low to moderate eccentricity (Milani et al. 2010). This family was chosen because it has a relatively small geocentric distance such that the majority of the population was expected to be visible within the limiting magnitude, and it is thought to be a very dynamically active population. Surrounding the Hungarias are dynamically unstable boundaries with a strong perihelion resonance with Jupiter, the node of the orbit locked to the node of Saturn, and an interac-

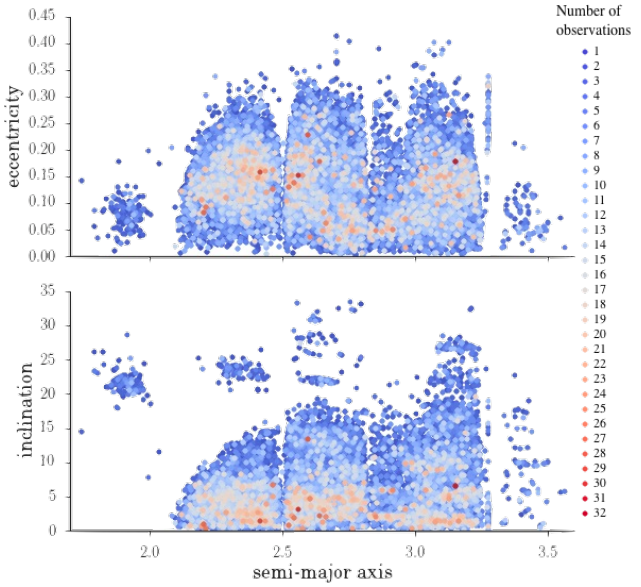

Figure 3. The number of observations of asteroids in the OSSOS data set organized by inclination and eccentricity as a function of semi-major axis. The majority of observations are in the regions with a larger population of asteroids. Axis labels could not be enlarged due to limitations in the plotting software.

tion with the orbit of Mars. As the region is populated by bodies thought to be native to the region, and as a result of collisional interactions of large parent bodies (Milani et al. 2010), it is possible that ongoing collisions could still reveal submerged volatile content. However, due to the low semi-major axis, it is likely that any exposed water ice would dissipate quickly. The second group consists of 3 known AAs which were observed by OSSOS, however their current state of activity is unknown. An lastly, we include images of a unreported comet during its period of activity discovered in the Canada-France Ecliptic Plane Survey (CFEPS) survey are also included to ensure that our pipeline can accurately identify a coma with reasonable certainty.

From calculated arcs provided by the Solar System Object Image Search (SSOIS) ephemeris (Gwyn et al. 2012) of 671,234 main belt objects in the Asteroids Dynamic Site (AstDys) catalogue (Agency et al. 2015), a prediction can be made as to which asteroids are present in the OSSOS data set and are able to be examined for cometary activity. With a data set of 3,528 images from the OSSOS, there were found to be 201,477 observations in the r band of 46,367 asteroids. For the purposes of our search it was important to be able to predict which objects were observed, and as such only numbered asteroids where the arcs are relatively well calculated with sub-arcsecond uncertainties were considered.

Of the selected test groups there were found to be 76 observations of 25 asteroids within a population of 1187 Hungarias, 11 observations of previously discovered AAs (3 of 238P/Read, 6 of P/2012 F5 (Gibbs), and 2 of (2201) Oljato), and 3 observations of the CFEPS comet.

From a set of 3,528 images, there were found to be 201,477 observations in the r band of 46,367 objects in the OSSOS data. A small group of objects in the Hungaria family, each of the previously identified AAs, and a comet during a period activity discovered in the CFEPS survey (unreported), are analyzed as our test cases for our automated pipeline. Of the 1187 Hungarias there are 76 observations of 25 objects; of the known AAs there are 11 observations: 3 of 238P/Read, 6 of P/2012 F5 (Gibbs), and 2 of (2201) Oljato; and 3 observations of the CFEPS comet.

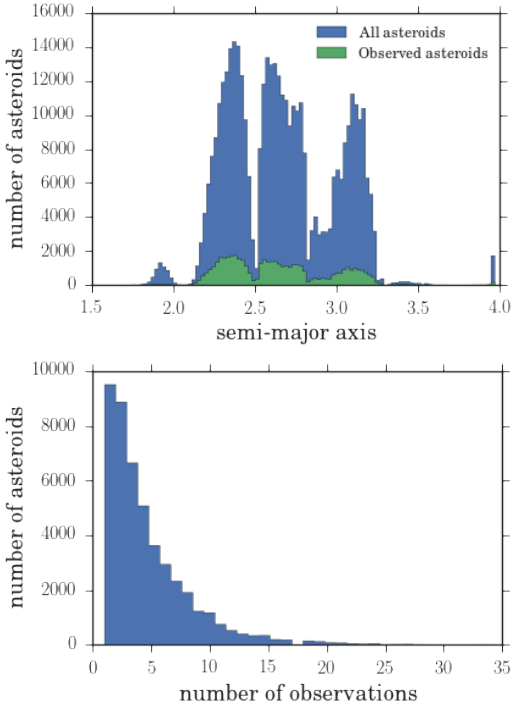

Figure 4. Top: The number of asteroids and observed asteroids in the main asteroid belt as a function of semi-major axis. The asteroid population is well represented by the OSSOS data set in terms of the population-weighted dynamical sample. Bottom: The distribution of multiple observations by the OSSOS of each asteroid observed at least once. Axis labels could not be shown due to limitations in the plotting software.

To determine the presence of activity, each object was examined photometrically for anomalous flux in the encompassing region indicative of a coma and/or tail. This was accomplished through measuring the point spread function (PSF) of the object, calculating the brightness profile, and comparing the profile to that of a star. The first step in this process is obtaining the precise location of the object in the image. This is complicated by the large uncertainties in the asteroid arcs such that calculated coordinates often are not accurate. It is therefore necessary to establish a set of criteria to be able to identify the asteroid in the image.

3.1. *Object identification*

An automated pipeline was written to identify each asteroid in an OSSOS exposure by: location relative to the predicted coordinates, elongation due to trailing effects resultant of the apparent rate of motion over the duration of the exposure, and apparent magnitude.

The coordinates of each object in the exposure were obtained from the photometric software SEP, and objects which were closest to the predicted location (at the midpoint of the exposure) as calculated by known arc (Chamberlin et al. 1997) were chosen as candidate ob-

jects. If no objects were detected within a set radius calculated from the uncertainty in the asteroid arc, the radius was increased by a factor of 1.5 and the search was repeated.

The predicted elongation of the trail was calculated from the motion of the asteroid over the length of the exposure under the assumption of constant motion. This was compared to the fitted PSF shape measured by SEP for each candidate object. A difficulty in this process is that objects which move faster during the exposure, and thus have longer trails, will be less elliptical in shape. As the photometry software is optimized for point sources and extended sources such as galaxies, the accuracy of the parameters describing the fitted PSF shape is expected to be correlated to the extent of the elongation. For this reason an uncertainty of 20 percent is assumed for the elongation, with the expectation that only objects which are markably inconsistent would be rejected. For very extended trails, with a ratio of semi-major axis to semi-minor axis of 5:1, SEP incorrectly resolves the asteroid as two separate objects. This is a result of an inconsistent flux distribution over the trailed asteroid, possibly a result of rotational or reflective effects (see figure 5). In this case the asteroid would require visual inspection. This process could be significantly improved with the inclusion of a trail fitting algorithm in the photometry software (see recommendations for a more detailed discussion).

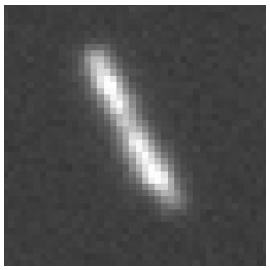

Figure 5. A fast moving asteroid trailed over the duration of the exposure with an uneven flux distribution over its length. This object required visual inspection as it was incorrectly resolved as multiple objects by SEP.

The inability of the photometry software to correctly measure the shape of the asteroid trail would also affect the accuracy of the flux measurement as the aperture may not include the total amount of light. As the centre of the object is determined by the flux weighted barycenter of the object (Bertin and Arnouts 1996), this may also result in an inaccurate measurement of the astrometry. In order to avoid this error, the centre coordinates of the object were chosen as the centre of the elliptical aperture for fast-moving objects. In addition, the elongation effect in itself may affect the accuracy of the flux measurement without taking into account the potential loss of light. This is a result of the flux being spread over a larger area than the point spread function (PSF), which reduces the per unit area apparent magnitude and the signal-to-noise (Vereš et al. 2012). A direct consequence is a lowered limiting magnitude for fast moving asteroids. A third consideration is that objects which are active and have jets or a coma will appear brighter than the expected magnitude calculated from previous observations. Depending on the extent of the activity, this could cause the object to be measured as several magnitudes greater than predicted. For these reasons, in subjecting the candidate object to a consistency check with the predicted value an uncertainty of 2 magnitudes was chosen (unless the object was predicted to vary by a larger amount in the span of 10 days following the exposure) and did not reject the object if it was inconsistent.

In order to accurately measure the PSF of the asteroid it is necessary to ensure that the asteroid is isolated from other sources. A catalogue of bright sources Bannister et al. (2015) built for the OSSOS data set from a collection of exposures taken under photometric conditions was used to ensure that the asteroids were not involved with a background source. The asteroid was rejected as involved if the centre-point of a background source was within 2.5 times the FWHM of the asteroid.

A candidate object which did not meet any of the criteria mentioned above was examined visually. Objects which met the location and elongation conditions were preferentially selected over those that only met the location and magnitude conditions. If multiple objects met the same level of criteria, they would also be examined visually.

Applying this identification process left 69 exposures of 21 objects to be examined.

Table 1
Reasons for rejection or visual inspection for images which could not be identified by the above criteria.

Total number of images	90
Rejection cause	**# images**
Involved with a background source	1
Not in the exposure or on the edge of the CCD	5
In saturated/diffraction region of a bright star	2
Bad exposure	4
Cause for visual inspection	**# images**
Incorrectly resolved as multiple objects	7
Did not meet any criteria condition	2
Retained	69

3.2. *Rejection causes*

If the asteroid flux information was lost in the exposure it was not visually inspected. This would be as result of the following reasons:

Involved with a background source:
When compared with a catalogue of bright sources the object was found to spatially coincide with a background object. As the catalogue was built from a set of exposures with photometric conditions, asteroids present in those exposures were incorrectly identified as involved. However, not included in the catalogue are dim sources, transient objects, and bad pixels/columns. In the case of the asteroid being involved with such objects, the photometry software would measure the convolved sources, and the elongation and magnitude would be inconsistent with the predicted values. If the background object were dim enough that the convolved source passed the magnitude condition, the PSF would be beyond the 5 sigma deviation, and the involvement would be caught by visual inspection. An example of

such a case is shown in figure 6.

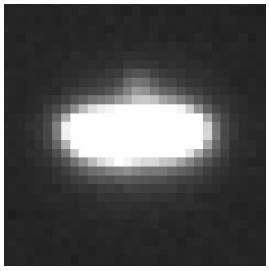

Figure 6. An asteroid involved with a dim background object. It is apparent that the bright feature is not a jet as it does not follow the direction of the trailing.

Not in the exposure or on the edge of the CCD:
If the SSOIS query incorrectly identified that an asteroid was on in an OSSOS exposure no object would be found at the predicted location as it would not be on the CCD. This is a result of the SSOIS reporting an observation if any part of the uncertainty ellipse of the arc overlaps the CCD, without taking into account the overscan region on the CCD edge.

In saturated/diffraction region of a bright star:
For objects close to but not involved with bright sources, the asteroid may in the diffraction region of the saturated pixels. This would result in the object not being detected within the uncertainty ellipse around the predicted co-ordinates as its PSF was obscured.

Bad exposure:
Exposures which were marked as bad due to loss of tracking, poor image quality, or were corrupted were rejected as the photometric information was not accurate.

3.3. *PSF profile comparison*

A postage stamp cutout of the asteroid of size two-and-a-half times the full-width-half-maximum (FWHM) and centred on the midpoint of the elongated shape was rotated such that asteroid trail was aligned parallel to the pixel rows on the CCD chip. The brightness profile was calculated by averaging the flux of the asteroid PSF over the length of the postage stamp. A stellar model PSF corresponding to the pixel location and magnitude of the asteroid on the CCD was obtained from the OSSOS processing software. A brightness profile of the model star was calculated by the rotated and flux averaged PSF, and interpolated to correspond the same pixel values as the asteroid profile.

Due to saturation effects, asteroids brighter than 18.5 magnitudes were not analyzed for activity by this process, but instead inspected visually. As a stellar model PSF has not, at the present time, been built for each OSSOS exposure, those without were also inspected visually.

As asteroids are point sources which exhibit bare photometric properties, the brightness profile of an inactive asteroid should be equivalent to that of a star. The presence of activity would therefore be indicated by discrepancies in the two profiles. The deviation between the profiles can be calculated through the subtraction of the ratio of each point to that of the mean, and comparing the residual to the measured uncertainty, as follows in the equation,

$$r - \bar{r} > n \cdot \sigma$$

where r is the ratio, $\bar{r}$ is the mean ratio, σ is the Poisson uncertainty, and n is integer multiple chosen as the lower limit for a detection of significant deviation between the profiles.

Profiles of an asteroid not indicating activity and that of the CFEPS comet are shown in figure 7. A lower limit of 3 sigma was chosen to indicate the presence of additional flux around an object, with the expectation that at least 1 percent of the population would be above this limit. Each asteroid with at least two pixels with greater than this limit were then visually examined for asymmetric features (such as would result from a jet) and extended wings (such as would result from a coma) when compared visually to the stellar model profile.

Table 2
Reasons that the brightness profile could not be calculated.

Retained from identification process	69
Cause for visual inspection	**# images**
Above 18.5 magnitude	2
No stellar model	14
Retained	53

Of the 50 images where the brightness profile was measured, 3 asteroids were found to have a 3 sigma deviation from the stellar model profile. Each of these objects were visually inspected and found to be overlapping the CCD edge, involved with saturated pixels causing the PSF to appear extended, or an incorrect identification of the asteroid. This included the previously discovered asteroids indicating that none were active during the time of their observation. Each exposure of the CFEPS comet was found to deviate by greater than 5 sigma.

The asteroids whose astrometry could not be precisely measured or could not be directly compared to a stellar model were examined visually for interesting features such as extended wings when compared with nearby stars in the same exposure (as in Hsieh and Jewitt 2006). Although this process is subjective, the intention was to select objects with distinct anomalies in the PSF at with at least 50 percent greater flux counts than the stars. Of the 25 images of the asteroids which were visually inspected, no activity was apparent.

4. RESULTS

4.1. *Assumed uncertainties for identification criteria*

The given uncertainty of 20 percent was found to be a reasonable choice as the percent difference between the predicted and measured elongations for the sample group of asteroids correctly measured by SEP was under 18 percent, and with a mean of 8 percent. This was therefore a good value for only rejecting cases where the elongation was markedly wrong. In only one case was it found that a background object was incorrectly selected as the asteroid due to its similar shape, location, and magnitude,

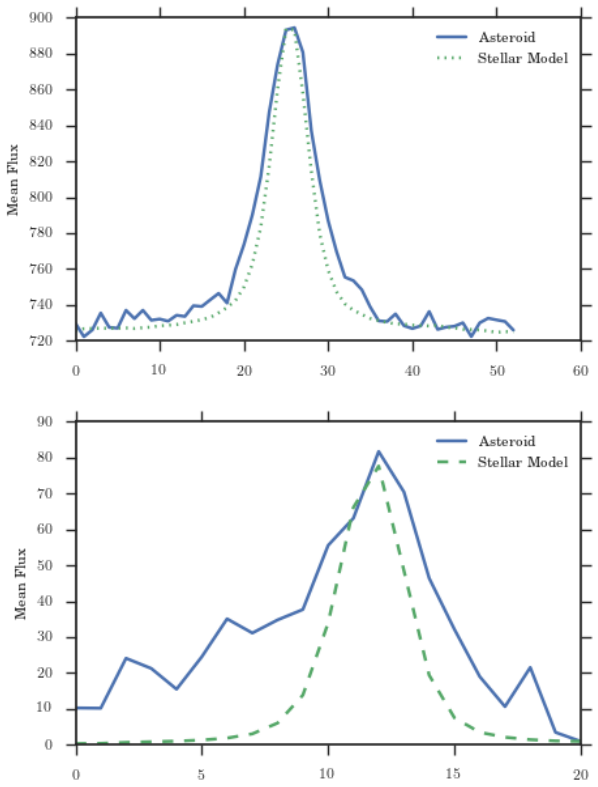

Figure 7. Top: A brightness profile of an asteroid is shown as a blue solid line, and that of the stellar model is shown as a green dashed line. The asteroid profile shows little deviation from the stellar profile, indicating bare photometric properties, and that no activity is present. Bottom: A brightness profile of the CFEPS comet is shown as a blue solid line, and that of the stellar model is shown as a green dashed line. An obvious flux difference is apparent in the wings of the profile indicating the presence of dust or ice surrounding the object. The comet in this case was observed at an angle to the sun resulting in a non-symmetric PSF.

and the asteroid being significantly elongated resulting in a higher uncertainty. This error was discovered as a result of the PSF not being characteristic of an asteroid where it was flagged for visual inspection.

Despite the expectation that the elongation was correlated to the inaccurate measurement of the magnitude due to the spread of the flux, no statistical relationship was found between the difference of the predicted and measured magnitude and the elongation, as calculated by an unpaired T-test. However, in a visual comparison with stellar model PSF constructed with the same magnitude as the asteroid as reported by SEP, the flux amplitudes were clearly and consistently dissimilar by an average difference of 0.3 mag. As the amplitude of the stellar model profile is only a scaling factor, this will not affect the test by which calculates the deviation of the residuals. This observation does lend suspicion on the photometry measurement, where the error could still be attributed to the flawed elliptical approximation of the trailed asteroids.

4.2. *Success of the search pipeline*

Of the original 90 exposures 12 were rejected as the asteroid PSF could not be measured and 25 could not be compared to the stellar model profile, leaving 53 asteroids (59%) of the original sample to be tested for activity the the developed pipeline. In order to calculate an estimate of the actual efficiency of the developed pipeline, only the cases where it was possible for each asteroid to be compared to the stellar profile were considered, leaving 62 exposures; of these, 53 asteroids (85.4%) were able to be tested. Of those which were not tested, 7 (11.2%) were incorrectly resolved as multiple objects, and 2 (3.2%) did not meet either the elongation or magnitude condition. In both cases this was a result of SEP being unable to characterize very extended trails. With an improved method of measuring the PSF of trailed objects it is expected that these statistics will be significantly improved.

Visual inspection was required for 28 (31.1%) of the original test sample. Of this group, 2 were beyond the saturation limit such that a comparison with the stellar model could not be made, 14 did not yet have a stellar model available, and 12 were rejected as the PSF could not be determined. With the upcoming OSSOS data release it is expected that the exposures which have not yet been processed by the OSSOS pipeline will be soon, and the stellar models will be available. Taking this into account the rejection rate for this study is 15.5%.

4.3. *PSF profile test*

There were 50 exposures where the object PSF profile was compared to a stellar model. Of these, 3 asteroids were found to deviate by over 3 sigma, and all 3 of the comet observations were found to deviate by over 5 sigma. Through a visual inspection of the profiles however, it is obvious that the method by which we calculate the deviation is insufficient. At present, the measurement of the average ratio (by which we subtract each pixel pair ratio and compare to the uncertainty) is calculated across the entire profile excluding the 4 greatest outliers. However, when there is significant deviation in the wings of the asteroid PSF, the average ratio is biased to agree with the deviation. The method could be improved by measuring the average ratio from only the central core pixels of the profiles, as the ratio should not be effected by the presence of activity. This issue has not been resolved, as the uncertainties of the wings of the profile are large enough to not meet even the lowest detection limit of 3 sigma, despite being visually detected to be significantly dissimilar to the stellar profile. This is currently an area of active development.

5. RECOMMENDATIONS FOR FUTURE DEVELOPMENT

The photometry software used (SEP) is optimized for point sources and extended sources such as galaxies which are approximated as ellipses. As the asteroids in our exposures can be trailed to a large extent such that the shape is less elliptical, it expected that the accuracy of the photometry is correlated to the extent of the trailing. As the astrometry is measured from the barycentric flux of the object (Bertin and Arnouts 1996), the uncertainties associated with the photometry result in additional errors. An attempt to minimize this effect was made through measuring the astrometry from the parameters describing the fitted PSF shape of the object rather than from a peak flux. This also fails, however, for objects which are extended to such a degree and/or have an uneven flux distribution across the trail such

that the approximated ellipse is no longer centred on the midpoint of the trail. The photometry, and as a result the astrometry, could be improved by a factor of 3 times for objects extended past 10 pixels with the inclusion of a trail fitting function such as is developed by Vereš et al. (2012). It is recommended that a trail fitting function be used to measure the PSF of object where the elongation is expected to extend past a ratio of 2:5 semi-minor to semi-major axis.

Two cases were found where the asteroid was not directly involved with a background source but were too faint to be detected by SEP as a result of being in a diffraction region of a bright source. In order to better differentiate this situation from objects which are not detected as a result of being on the edge of the CCD or not on the exposure, it is suggested that the involvement survey take into account FWHM of the background source. It would then be possible to reject cases where the object were too close to a bright source that the PSF could not be measured accurately despite a small angle difference on the exposure.

Comets and AAs alike are known to exhibit both coma and/or tails. A more rigorous search for tails could be implemented with an analysis of the variation in flux surrounding the object as a function of angle with respect to the trailing axis such as is done by Sonnett et al. (2011). Although it is expected that the tails would alter the asteroid PSF enough to result in a 3 sigma deviation from the stellar model, it may be that the tail is too faint with respect to the peak asteroid PSF to be detectable by this method.

Several of the AAs are dynamically and morphologically associated with asteroid families formed through collisional processes. For example 133P/Elst-Pizarro, 176P/(118403) LINEAR, 238P/Read, and 288P/(300163) 2006 VW_{139} are believed to be related to the Themis family, P/2010 A2 (LINEAR) and 311P/PANSTARRS (P/2013 P5) with the Flora family, and P/2012 T1 (PANSTARRS) and 313P/Gibbs (2014 S4) with the Lixiaohua family (Jewitt et al. 2015; and references therein). It cannot be assumed that there is a causal link between family membership and the probability of being active, however, given the number of asteroids which populate these families. Three AAs (133P/Elst-Pizarro, 288P/(300163) 2006 VW_{139}, and P/2012 F5 (Gibbs)) have also been linked to young asteroid clusters where it may be expected that recent collisions have exposed previously submerged volatiles. Depending on the cause of the activity, whether it is a result of sublimation or collisions, it would be expected that more than one object would share the same properties as the discovered AA. Despite that the AAs in general have been found to have widely varying orbital dynamics, it would be prudent to begin searching for objects in the OSSOS data set where AAs have been previously discovered.

The pipeline developed in this study is available open-source (https://github.com/k-a-webb/MainBeltComets). It will be used in future (with the photometry-fitting improvements suggest above) to process OSSOS data for asteroid measurements as the survey continues through 2016.

6. SUMMARY

1. A technique was developed to identify the precise location of asteroids in the OSSOS data set by their predicted location as calculated by the respective arc, elongation of the trail which results from the motion of the asteroid during the exposure, and apparent magnitude. A comparison was made with a catalogue of bright background sources to reject cases of involvement. Cases where no object or multiple objects met the appropriate criteria conditions were rejected and instead visually inspected.

2. The PSF of the asteroids which could be identified by the above method were averaged along the direction of motion and a brightness profile was measured. The relationship of the asteroid profile with a stellar model profile was analyzed for residuals above a lower limit of 3 sigma. No AA candidates were identified in the chosen test sample. Each CFEPS comet was found to deviate from the stellar model profile by more than 5 sigma.

3. From the test sample of 90 exposures of the Hungarias, previously discovered AAs, and the CFEPS comet 12 (13.3%) exposures were rejected as the PSF could not be measured, 9 (10%) as the asteroid PSF did not meet the identification criteria conditions, 2 (2.2%) due saturation effects such that the brightness profile could not be measures, and 25 (27.8%) due to a lack of stellar model to compare the asteroid profile against.

4. Considering only the cases where it was possible to measure the asteroid PSF and compare it to a stellar model there were 62 observations. With the rejection of 9 (14.5%) of the asteroids as described above, 53 (85.4%) were retained.

ACKNOWLEDGEMENTS

I would like to thank Dr. Michele Bannister of the National Research Council (NRC) of Canada Hertzberg Institute of Astrophysics (HIA) for their help in the developing the search pipeline, Dr. J.J. Kavelaars of the HIA for assistance with accessing the Canadian Astronomy Data Centre and for providing the CFEPS comet images. This work is supported in part by the NRC HIA and the University of Victoria, and is based on observations obtained with MegaCam, a joint project of CFHT and CEA/DAPNIA which is operated by the NRC of Canada, the Institut National des Science de l'Univers of the Centre National de la Recherche Scientifique (CNRS) of France, and the University of Victoria.

REFERENCES

European Space Agency, SpaceDys, and and University of Pisa Astronomical University of Belgrade. Asteroids - dynamic site. 2015. URL http://hamilton.dm.unipi.it/astdys.

M. Bannister, B. Gladman, J. Kavelaars, J.-M. Petit, S. Gwyn, and Y.-T. Chen. The Outer Solar System Origins Survey: design and first-quarter discoveries. *Astrophysical Journal Supplements*, 2015.

K. Barbary and contributers. Source extraction and photometry in python. 2015. URL http://sep.readthedocs.org/.

E. Bertin and S. Arnouts. SExtractor: Software for source extraction. A&AS, 117:393–404, jun 1996. doi:10.1051/aas:1996164.

A. B. Chamberlin, D. K. Yeomans, P. W. Chodas, J. D. Giorgini, R. A. Jacobson, M. S. Keesey, J. H. Lieske, S. J. Ostro, E. M. Standish, and R. N. Wimberly. JPL Solar System Dynamics WWW Site. In *AAS/Division for Planetary Sciences Meeting Abstracts #29*, volume 29 of *Bulletin of the American Astronomical Society*, page 1014, jul 1997.

E. W. Elst, O. Pizarro, C. Pollas, J. Ticha, M. Tichy, Z. Moravec, W. Offutt, and B. G. Marsden. Comet P/1996 N2 (Elst-Pizarro). IAU Circ., 6456:1, aug 1996.

F. P. Fanale and J. R. Salvail. The water regime of asteroid (1) Ceres. Icarus, 82:97–110, nov 1989. doi:10.1016/0019-1035(89)90026-2.

A. M. Gilbert and P. A. Wiegert. Searching for main-belt comets using the Canada-France-Hawaii Telescope Legacy Survey. Icarus, 201:714–718, jun 2009. doi:10.1016/j.icarus.2009.01.011.

S. D. J. Gwyn, N. Hill, and J. J. Kavelaars. SSOS: A Moving-Object Image Search Tool for Asteroid Precovery. PASP, 124:579–585, jun 2012. doi:10.1086/666462.

H. H. Hsieh and D. Jewitt. A Population of Comets in the Main Asteroid Belt. *Science*, 312:561–563, apr 2006. doi:10.1126/science.1125150.

H. H. Hsieh, L. Denneau, R. J. Wainscoat, N. Schörghofer, B. Bolin, A. Fitzsimmons, R. Jedicke, J. Kleyna, M. Micheli, P. Vereš, N. Kaiser, K. C. Chambers, W. S. Burgett, H. Flewelling, K. W. Hodapp, E. A. Magnier, J. S. Morgan, P. A. Price, J. L. Tonry, and C. Waters. The main-belt comets: The Pan-STARRS1 perspective. Icarus, 248:289–312, mar 2015. doi:10.1016/j.icarus.2014.10.031.

D. Jewitt, H. Hsieh, and J. Agarwal. The Active Asteroids. *ArXiv e-prints*, feb 2015.

J. X. Luu. High resolution surface brightness profiles of near-earth asteroids. Icarus, 97:276–287, jun 1992. doi:10.1016/0019-1035(92)90134-S.

A. Milani, Z. Knežević, B. Novaković, and A. Cellino. Dynamics of the Hungaria asteroids. Icarus, 207:769–794, jun 2010. doi:10.1016/j.icarus.2009.12.022.

D. Prialnik and E. D. Rosenberg. Can ice survive in main-belt comets? Long-term evolution models of comet 133P/Elst-Pizarro. MNRAS, 399:L79–L83, oct 2009. doi:10.1111/j.1745-3933.2009.00727.x.

S. S. Sheppard and C. Trujillo. Discovery and Characteristics of the Rapidly Rotating Active Asteroid (62412) 2000 SY178 in the Main Belt. AJ, 149:44, feb 2015. doi:10.1088/0004-6256/149/2/44.

S. Sonnett, J. Kleyna, R. Jedicke, and J. Masiero. Limits on the size and orbit distribution of main belt comets. Icarus, 215: 534–546, oct 2011. doi:10.1016/j.icarus.2011.08.001.

P. Vereš, R. Jedicke, L. Denneau, R. Wainscoat, M. J. Holman, and H.-W. Lin. Improved Asteroid Astrometry and Photometry with Trail Fitting. PASP, 124:1197–1207, nov 2012. doi:10.1086/668616.